



HAL
open science

Glow in the dark: use of synchrotron μ XRF trace elemental mapping and multispectral macro-imaging on fossils from the Paris Biota (Bear Lake County, Idaho, USA).

Arnaud Brayard, Pierre Guériaux, Mathieu Thoury, Gilles Escarguel, Kevin G. Bylund, Emmanuel Fara, Nicolas Goudemand, James F. Jenks, Laurel J. Krumenacker, Nicolas Olivier, et al.

► To cite this version:

Arnaud Brayard, Pierre Guériaux, Mathieu Thoury, Gilles Escarguel, Kevin G. Bylund, et al.. Glow in the dark: use of synchrotron μ XRF trace elemental mapping and multispectral macro-imaging on fossils from the Paris Biota (Bear Lake County, Idaho, USA).. *Geobios*, 2019, 54, pp.71-79. 10.1016/j.geobios.2019.04.008 . hal-02168490

HAL Id: hal-02168490

<https://hal.science/hal-02168490>

Submitted on 25 Oct 2021

HAL is a multi-disciplinary open access archive for the deposit and dissemination of scientific research documents, whether they are published or not. The documents may come from teaching and research institutions in France or abroad, or from public or private research centers.

L'archive ouverte pluridisciplinaire **HAL**, est destinée au dépôt et à la diffusion de documents scientifiques de niveau recherche, publiés ou non, émanant des établissements d'enseignement et de recherche français ou étrangers, des laboratoires publics ou privés.



Distributed under a Creative Commons Attribution - NonCommercial 4.0 International License

Glow in the dark: use of synchrotron μ XRF trace elemental mapping and multispectral macro-imaging on fossils from the Paris Biota (Bear Lake County, Idaho, USA) *

Arnaud Brayard ^{a,*}, Pierre Gueriau ^{b,c}, Mathieu Thoury ^b, Gilles Escarguel ^d, the Paris Biota Team [†]

¹ Biogéosciences, UMR6282, CNRS, Université Bourgogne Franche-Comté, 6 Boulevard Gabriel, 21000 Dijon, France

² Ipanema, CNRS, ministère de la culture, UVSQ, USR3461, Université Paris-Saclay, F-91192 Gif-sur-Yvette, France

³ Anom Lab, Institute of Earth Sciences, University of Lausanne, CH-1015 Lausanne, Switzerland

⁴ Univ. Lyon. Laboratoire d'Ecologie des Hydrosystèmes Naturels et Anthropisés, UMR 5023 CNRS, Université Claude Bernard Lyon 1, ENTPE. F-69622 Villeurbanne Cedex, France

[†] The Paris Biota Team includes, in alphabetical order: Arnaud Brayard (team leader; Biogéosciences, Univ. Bourgogne Franche-Comté, Dijon, France), Kevin G. Bylund (Spanish Fork, UT, USA), Gilles Escarguel (LEHNA, Univ. Lyon 1, Lyon, France), Emmanuel Fara (Biogéosciences, Univ. Bourgogne Franche-Comté, Dijon, France), Nicolas Goudemand (IGFL, ENS-Lyon, Lyon, France), Pierre Gueriau (Synchrotron SOLEIL, Gif-sur-Yvette, France/Institute of Earth Sciences, University of Lausanne, Swiss), James F. Jenks (West Jordan, UT, USA), L.J. Krumenacker (Idaho Museum of Natural History, Idaho State Univ., Pocatello, ID, USA), Nicolas Olivier (Magmas et Volcans, Univ. Clermont Auvergne, Clermont-Ferrand, France), Daniel A. Stephen (Dpt. of Earth Sciences, Utah Valley Univ., Orem, UT, USA), Christophe Thomazo (Biogéosciences, Univ. Bourgogne Franche-Comté, Dijon, France), Mathieu Thoury (IPANEMA, Univ. Paris-Saclay/Synchrotron SOLEIL, Gif-sur-Yvette, France), and Emmanuelle Vennin (Biogéosciences, Univ. Bourgogne Franche-Comté, Dijon, France).

* Corresponding author. E-mail address: arnaud.brayard@u-bourgogne.fr (A. Brayard).

* Corresponding editor: Emmanuel Fara.

Abstract

The end-Permian mass extinction is the largest global-scale event ever recorded; it also corresponds to the expansion of the Modern Evolutionary Fauna, which will lead to present-day ecosystems. The Early Triassic is thus a pivotal interval in the evolution of many marine groups. An exceptionally well-preserved early Spathian fossil assemblage, the Paris Biota, was recently discovered in southeastern Idaho, USA; it represents the earliest complex marine ecosystem known to date for the post-crisis aftermath. Here we use synchrotron μ XRF imaging to retrieve further anatomical, paleobiological and taphonomical data on some of the most intriguing fossils from the Paris Biota, such as contours of the central disc and the full length of arms in an ophiuroid specimen. We also show that multispectral macro-imaging is powerful to reveal or enhance the visualization of some specimens, particularly shrimps, that are barely perceptible under visible and UV lights. The complementary use of both techniques suggests that the actual richness and abundance of organisms in this exceptionally well preserved Early Triassic ecosystem is likely to remain underestimated, and this situation may be even worse in other less well preserved spatiotemporal contexts.

Keywords:

Early Spathian

Early Triassic

Paris Biota

Synchrotron μ XRF mapping

Multispectral macro-imaging

1. Introduction

The end-Permian mass extinction, *ca.* 252 Ma, is the most devastating global-scale event ever recorded, resulting in the loss of more than 80% of all marine species and the disappearance of typical Paleozoic clades. The Permian/Triassic (PT) boundary therefore corresponds to a pivotal time interval marking the end of the dominance of the Paleozoic

Evolutionary Fauna and the expansion of the Modern Evolutionary Fauna (Vermeij, 1977; Raup, 1979; Gould and Calloway, 1980; Sepkoski, 1981). Recovery from the PT crisis is usually assumed to be a long and delayed process spanning at least the entire Early Triassic (*ca.* 5 myr; e.g., Chen and Benton, 2012). Recurrent marked changes in water temperature, large-scale fluctuations of the global carbon cycle, and various harsh marine conditions are indeed documented for the Early Triassic (e.g., Payne et al., 2004; Galfetti et al., 2007; Grasby et al., 2013; Goudemand et al., in press; Thomazo et al., in press). However, the post-crisis biotic recovery was much shorter for at least some nektonic-pelagic groups such as ammonoids and conodonts (Orchard, 2007; Brayard et al., 2009). Such discrepancies highlight the fact that the links between Early Triassic environmental variations and the recovery of marine ecosystems still remain poorly understood.

Recently a new, exceptionally well preserved Early Triassic (*ca.* 1.3 myr after the PT boundary) fossil assemblage was discovered in lowermost Spathian rocks of southeastern Idaho, USA: the Paris Biota (Brayard et al., 2017). It represents the most complex marine ecosystem known to date for the Early Triassic, with more than 20 metazoan orders including sponges, brachiopods, mollusks, arthropods, echinoderms, and vertebrates (Brayard et al., 2017, 2019; Doguzhaeva et al., 2018; Botting et al., 2019; Charbonnier et al., 2019; Romano et al., 2019; Saucède et al., 2019; Thuy et al., 2019). Most unexpectedly, basal sponges previously known only from the early Paleozoic (i.e., a 200-myrr Lazarus taxon; Botting et al., 2019) are found together with gladius-bearing coleoid cephalopods, a common and diversified group expected to originate in the Jurassic (i.e., more than 50 myr after the Early Triassic; Brayard et al., 2017; Doguzhaeva et al., 2018).

The Paris Biota thus stands as a key fossil ecosystem in the wake of the PT mass extinction. However, many of the sampled specimens still remain to be formally described, a long and difficult task as some of them require very cautious manual preparation to access anatomical structures hidden in the sedimentary matrix and critical for taxonomic identification and paleobiological interpretation. Unfortunately, X-ray micro-tomography, which is now routinely used to extract virtually fossils from their rocky or amber coffins (e.g., Tafforeau et al., 2006; Sutton, 2008; Garwood et al., 2012; Jauvion et al., 2016; Moreau et al., 2017), so far failed to reveal such hidden anatomical features in the Paris Biota, as traditional tomography suffers from a physical limit due to the extremely high difference in X-ray absorbance in different directions of such flattened fossils. Here we attempt to retrieve key anatomical, paleobiological and taphonomical data on some of the most important fossils (echinoderms, crustaceans) from the Paris Biota by using two innovative non-destructive

methods: (i) synchrotron micro X-ray fluorescence (μ XRF) major-to-trace elemental mapping, and (ii) multispectral macro-imaging (see also Saucède et al., 2019 and Thuy et al., 2019 for additional illustrations). These fossils have been selected because: (i) they are known only from the Paris Biota, (ii) they display an excellent state of preservation, (iii) they belong to different clades with different preservation type, and (iv) they are often abundant (e.g., crustaceans; Brayard et al., 2017). These features make these specimens an appropriate basis to explore the various potential taphonomical pathways and elemental replacements that occurred during the fossilization processes of the Paris Biota. Synchrotron μ XRF mapping of heavy elements such as strontium and yttrium has been shown to be of great promise to reveal fossil remains buried under fine layers of sediments (Gueriau et al. 2014, 2018). Multispectral macro-imaging constitutes a new (still under development) but very promising approach for paleontological material (see Thoury et al., 2016 for an application on archeological materials). Contrary to classical ultraviolet (UV) and visible photography or microscopy, it allows researchers to collect reflectance and luminescence images within spectra of a few nanometers or dozen of nanometers, ranging from the UV-A to the near-infrared (NIR) domain, thus greatly increasing the number of potential sources of morphological contrasts.

2. Methods

2.1. Synchrotron μ XRF mapping

2.1.1. General principles

This 2D imaging technique is based on a similar principle to elemental mapping under a scanning electron microscope (SEM-EDXS; see Iniesto et al., 2019 for applications on Paris Biota specimens), but instead of electrons (under the SEM), the emitted element-specific XRF photons are produced by bombarding the studied specimen with X-rays generated by a synchrotron light source. One main advantage is that synchrotron setups can accommodate large fossils (Bergmann et al., 2012) and are sensitive to trace elements up to the part per million level (Bergmann et al., 2010; Gueriau et al. 2014, 2015). Gueriau et al. (2018) described in details the principle of μ XRF as well as the advantages of using the synchrotron light, and they discussed data collection parameters and properties (e.g., detectable information depth, spatial resolution, acquisition time, excited elements).

2.1.2. Rationale of its application to the Paris Biota

Synchrotron μ XRF mapping was here applied to one ophiuroid, two crinoid, and seven crustacean specimens from the Paris Biota to investigate preferential major-to-trace elemental

incorporations within entire fossils. This approach was also used to look for tissue-specific trace heavy element incorporation (e.g., Pb, Sr, and Y), whose XRF emission lines offer important information depth (typically 200–400 μm in calcium phosphates and carbonates) and allow accessing anatomical features hidden under the sedimentary matrix covering the specimen (Gueriau et al., 2014, 2016, 2018).

Trace metals such as Fe, Cu and Zn, which are initially involved in biomolecules with specific biological functions (e.g., oxygen carriers, pigmentation) and have the potential to be preserved for millions of years in various fossils (Wogelius et al., 2011; Edwards et al., 2014) were also searched for. As many fossils from the Paris Biota are largely made of calcium phosphates (Brayard et al., 2017; Iniesto et al., 2019), special attention was given to rare earth elements (REE) that substitute Ca post-mortem in fossils (Gueriau et al., 2014, 2016). These elements are used: (i) as indicators of post-mortem changes that may have affected the fossil chemistry, thus altering the original biological signals (Reynard and Balter, 2014), and (ii) to infer paleo-seawater chemistry, redox and paleo-environmental conditions, as well as taphonomical processes (Gueriau et al., 2015).

2.1.3. Used setup

Synchrotron μXRF maps were collected at the DiffAbs beamline of the SOLEIL synchrotron (Gif-sur-Yvette, France), using a monochromatic beam of 18 keV, selected for excitation of K-lines from phosphorus to yttrium and L-lines from cadmium to uranium. In order to map the specimens with a high resolution, the beam was reduced down to a diameter of 50 μm using a molybdenum pinhole. Samples were mounted on a scanner stage allowing 90 mm movements and orientated at 45° to the incident beam and at 45° to the XRF detector, a four-element silicon drift detector (Vortex-ME4, Hitachi High-Technologies Science America, Inc.; total active area: 170 mm^2) placed in the horizontal plane. Thus, analyses of rather large specimens (up to *ca.* 90 \times 90 mm), with micrometer accuracy, were possible. μXRF elemental maps were produced through the collection of integrated intensities (sum of the four-elements XRF detector) in selected spectral regions of interest corresponding to emission from elements showing contrast between the fossil and its encasing and surrounding matrix.

2.2. Multispectral macro-imaging

2.2.1. General principles

Since the first tests in the 1920s (Simpson, 1926), comparisons of images obtained under visible light and UV-induced fluorescence are routinely used in paleontology as some fossil structures can sometimes be detected only under UV light (Tischlinger, 2001; Hone et al., 2010; Caze et al., 2011, 2015; Tischlinger and Arratia, 2013; Jattiot et al., 2015; Brayard et al., 2017). UV photography techniques have been considerably improved over the last decades, and high resolution composite images of specimens under both visible and UV lights can reveal very fine details unseen under visible light alone (e.g., Haug et al., 2009).

However, luminescence imaging has been mainly constrained by several factors. First, the choice of the excitation light is often mostly limited to the UV-A range due to: (i) the common available hardware, and (ii) the violet component of UV-A sources that can be easily filtered out so that the generated luminescence, often occurring in the visible range, can be detected by the naked eye or a RGB detector. Second, the spectral range and flux of the sources, such as available lamp sources, are generally sold with a low wattage and a wavelength restricted to *ca.* 250 nm, or more commonly to *ca.* 365 nm (Kaye et al., 2015). The detection modality is an additional key parameter: most of published works used a RGB detector (Caze et al., 2015; Falk et al., 2016) which provides a color image, but strongly limits the potential of associating specific emission with an anatomical part since the signal is only coded on three partially overlapping spectral channels. Overall, new imaging techniques based on the luminescence principles but using different wavelength emissions and thus, different illuminations, are promising (Kaye et al., 2015).

The technique of multispectral macro-imaging relies on collecting reflectance and luminescence images in distinct spectral ranges from the UV domain up to the NIR with the aim of collecting enhanced anatomical contrasts from both the specimen and between the specimen and the matrix. Here the fossil and its surrounding matrix are illuminated under different selected wavelengths from the UV up into the NIR thanks to LED lights. Each of these LED lights illuminates over a narrow spectral range and are easier to handle than several laser lights for a lower cost. The collection of images in specific spectral ranges is made using different transmission interferential filters positioned in front of the imaging setup composed of an apochromatic 60 mm lens coupled to a Si EM-CCD. The images collected under different illumination/detection couples can thus be associated to one of the channels associated with red, green and blue colors to generate false color images (Fig. 1). Different composite images can be generated, based on the selected illumination/detection couples and depending on the details to be highlighted. There is no general rule governing the selection of

illumination/detection couples as each studied specimen will yield his own response according to its type and state of preservation.

The use of multispectral macro-imaging up to the NIR in macrofossil photography remains rare (Sansone et al., 2017; Mapes et al., in press), contrary to IR that are utilized for determining and mapping organic or mineralogical composition (see Iniesto et al., 2019 for examples on specimens of the Paris Biota to characterize Ca-phosphate signatures using micro Fourier Transform IR analyses). However, such luminescence imaging can be explored with increasing ease by means of recent cameras with an improved sensitivity. By using such UV-to-NIR multispectral technique, we avoid many flaws inherent to traditional UV-light fluorescence methods that heavily relies on the used wavelength and filter. More importantly, we show that images under IR illumination and/or detection are also powerful to reveal hidden structures and details, and that combining images from different illumination and detection wavelengths can result in extremely informative pictures. Multispectral macro-imaging employed for Paris Biota specimens was applied to four slabs containing crustacean specimens (exemplified in Fig. S1, Appendix A) and to one ophiuroid and two crinoid specimens.

2.2.2. Used setup

The imaging system used to record the luminescence images is an innovative setup (a detailed description of the system is currently in preparation, including applications to a wide range of fossil specimens), which consists of a low-noise 1 megapixel Si EM-CCD camera (Qimaging Rolera EMC2) with a sensitivity ranging from 200 to 1100 nm. The camera is fitted with a UV-VIS-IR 60 mm 1:4 Apo Macro lens (CoastalOptics) in front of which is positioned a filter wheel holding 8 Interference band-pass filters (Semrock) to collect images in specific spectral ranges. Illumination was provided by 16 LED lights ranging from 365 up to 700 nm (CoolLED pE-4000), coupled to a liquid light-guide fiber fitted with a fiber-optic ring light-guide. This setup provides a homogeneous illumination of the region of interest. Resulting digital images are processed using ImageJ (stacking, image registration of the different couples, and production of false color RGB composites).

3. Results

3.1. Synchrotron μ XRF mapping

The strongest contrasts were observed in echinoderms and arise from the strontium (Sr) distribution, which is essentially confined to the skeletal calcite (Fig. 2; Saucède et al.,

2019). Strontium is indeed known to substitute for Ca up to several wt% in the crystal structure of Ca-based minerals, particularly calcium carbonates, as Sr ionic radius is close to that of Ca in these minerals (Gueriau et al., 2018). As Sr XRF photons can escape from a depth of 150–250 μm in such minerals (even more for a less-dense matrix), anatomic features hidden under a fine layer of sediment can be revealed (Gueriau et al., 2014, 2018). Incorporated traces of strontium that show up from below the sediment can provide much finer details of the general anatomy of some specimens, such as the contours of the central disc in ophiuroids (Fig. 2). More importantly, they also reveal: (i) previously hidden anatomical features, such as crinoid cirri with elements in connection (Saucède et al., 2019) and the full length of ophiuroid arms (Fig. 2), and (ii) unexpected additional specimens lying under the sediment surface (Saucède et al., 2019).

Crustaceans are preserved in calcium phosphate minerals (Brayard et al., 2017; Iniesto et al., 2019), which also incorporated strontium, as well as REE and yttrium (Y) that preferentially substitute for Ca in calcium phosphate (Gueriau et al., 2018). The distribution of Y, whose information depth is even greater than that of Sr, contributes to complement images obtained under visible and UV lights (Fig. 3). In a few fossils, trace metals appear concentrated in very localized places, which could somehow suggest the preservation of a specific organ, such as the digestive track of shrimps revealed by the distribution of Y (Fig. 3).

3.2. Multispectral macro-imaging

Some variations among and within groups can be observed as luminescence properties of fossils vary according to their mineralogical composition and preservation. Thus, comparisons belonging to different taxa can probably help deciphering specific influences of biological features from shared taphonomic pathways. Regarding Paris Biota specimens, echinoderms and crustaceans yielded interesting results both in terms of the application of this imaging technique and in terms of their anatomical study.

Crinoids and ophiuroids are preserved in calcite and show a strong luminescence only in the NIR (Fig. 4). This luminescence does not always reveal hidden characters under the sediment (but see Thuy et al., 2019). However, in most cases it improves details and provides contrasted images with more relief (Figs. 1, 4). This luminescence probably results from elements incorporated in calcite crystals and/or from the overall structuring (e.g., size, shape and orientation) of these crystals. More analyses are necessary to determine the actual origin

of this luminescence. Some specimens, or only parts of them, may not luminesce, suggesting the interplay of differential preservation pathways on this property.

Regarding crustaceans, and especially shrimps, composite pictures based on multispectral macro-imaging are highly contrasted. This likely results from the apatite composition of their carapace (Iniesto et al., 2019). Even in the case of poorly-preserved specimens, sometimes only represented by an extremely low relief and weakly fluorescing under classical UV light, multispectral macro-imaging clearly reveals the full extent of some specimens that could not be detected under visible light (Fig. 5(A, B)). Additionally, more anatomical details are visible on the specimens but also on the surrounding sediment such as isolated appendices or cuticle remains (Figs. 5(C, D), 6), making it easier to distinguish between close specimens. Since the remains of a single individual have the same luminescence properties, the use of a composite image developed under different illumination/detection wavelengths strongly enhances contrasts and makes it possible to highlight many more anatomical details and to provide information on certain internal structures (e.g., insertion of appendages, articulation among segments), which are hardly and not always discernable under visible and UV lights (Fig. 7).

4. Discussion

Synchrotron μ XRF and multispectral macro-imaging experiments on Paris Biota specimens successfully reveal new data on some fossils from this unique fossil ecosystem. Synchrotron μ XRF mapping has been used here only on crustaceans and echinoderms occurring in the Paris Biota. Several other organisms (e.g, brachiopods, mollusks, sponges) have yet to be analyzed. However, we have shown that this technique is useful for uncovering hidden specimens and particular anatomical features under the sediment (e.g., for echinoderms). Exploiting the 150-300 μ m information depth offered by μ XRF may nonetheless require some preparation (reduction, to such a thickness, of the covering matrix layer), and the size of the fossil to be analyzed in a single shot is limited to a few cm^2 in most synchrotrons, but reaches *ca.* $90 \times 90 \text{ mm}^2$ at DiffAbs-SOLEIL, and even $1000 \times 600 \text{ mm}^2$ at SSRL beamline 6-2 (Edwards et al., 2018). Data acquisition are also time-consuming when specimens are numerous or large, although the technique has been considerably improved over the last decade (Bergmann et al., 2010, 2012; Edwards et al., 2018; Gueriau et al., 2018). Trace elemental distributions may not always uncover new details in Paris Biota fossils, but reconstruction of REE patterns and other redox and paleo-environmental proxies through the quantification of trace elemental concentrations (Gueriau et al., 2014, 2015) should provide

new insights into taphonomical processes, including decay, burial and/or diagenesis conditions, such as local redox state, microbially-mediated mineralizations or recrystallization processes.

In comparison, signals provided by multispectral macro-imaging are restricted to the sample surface, but the wide range of illumination/detection wavelengths available strongly increases the possible sources of morphological contrasts. In terms of resolution, the macro-lens reveals fine details, as well as imaging specimens of varying sizes with high versatility and ease of use. Note that attaining such versatility has become an important goal at synchrotron XRF beamlines, e.g., SSRL beamline 6-2 developed a custom system allowing the X-ray spot size to be changed quickly and easily via different pinholes on a rotation stage (Edwards et al., 2018). The number of pixels of the camera being fixed, an important counterpart of such high-resolution imaging is the reduction of the field of view, so that fully imaging cm-large specimens requires the collection of a set of overlapping images that are later stitched. Multispectral macro-images are nonetheless collected very quickly as only a few minutes per sample position are needed, depending on the number of illumination/detection combinations to be acquired. Another advantage of multispectral macro-imaging is that, unlike synchrotrons, the work sessions do not rely on highly competitive calls for proposals. Yet, the setup used for this technique is presently only available at IPANEMA (Gif-sur-Yvette, France; ongoing development by one of us [M.T.]). Future improvements, particularly in the automation of filtering and image collection procedures, will contribute to a wider dissemination of this system.

Both complementary techniques show best results for echinoderms and crustaceans of the Paris Biota. In addition to the fact that these techniques lead to an improved description of the specimens, they also reveal that the number of specimens actually occurring in a given deposit is potentially much higher than that assessed by a simple visual count under visible and/or UV light. In the specific case of the Paris Biota, this implies that the real taxonomic richness and abundance of this remarkably well-preserved fossil assemblage may still be underestimated. Synchrotron μ XRF mapping and multispectral macro-imaging may be therefore useful to correct the observed diversity signal. They could also be used on other known Early Triassic assemblages from different environments, or on any other geological intervals, where they may be promising in revealing their real fossil contents. In the context of the Early Triassic recovery, for which taxonomic richness and individual abundances in local and regional assemblages are among key parameters to elaborate accurate macroevolutionary and macroecological scenarios, this study emphasizes that it will be of paramount importance

to intensify sampling efforts and to use such imaging methods regularly in a variety of locations and environments.

Appendix A. Supplementary information

Supplementary information (including Fig. S1) associated with this article can be found, in the online version, at:

Acknowledgements

We thank SOLEIL Synchrotron for provision of beamtime (project 20171046) and C. Mocuta for assistance at the DiffAbs beamline. This work is a contribution to the ANR project AFTER (ANR-13-JS06-0001-01) and was also supported by the French “Investissements d’Avenir” program, project ISITE-BFC (ANR-15-IDEX-03). We thank M. Iniesto for his comments on an earlier version of this work. We acknowledge the Bear Lake County road department and private land owner D. M. Clow (Ogden, Utah) for allowing access to studied exposures, as well as A.S. Grosjean, P. Guenser and T. Hurd for their help on the field.

References

- Bergmann, U., Manning, P.L., Wogelius, R.A., 2012. Chemical mapping of paleontological and archeological artifacts with synchrotron X-rays. *Annual Review of Analytical Chemistry* 5, 361–389.
- Bergmann, U., Morton, R.W., Manning, P.L., Sellers, W.I., Farrar, S., Huntley, K.G., Wogelius, R.A., Larson, P.L., 2010. *Archaeopteryx* feathers and bone chemistry fully revealed via synchrotron imaging. *Proceedings of the National Academy of Sciences, USA* 107, 9060–9065.
- Botting, J.P., Brayard, A., the Paris Biota Team, 2019. A late-surviving Triassic protomonaxonid sponge from the Paris Biota (Bear Lake County, Idaho, USA). *Geobios* 54, xxx–xxx.
- Brayard, A., Escarguel, G., Bucher, H., Monnet, C., Bruhwiler, T., Goudemand, N., Galfetti, T., Guex, J., 2009. Good genes and good luck: Ammonoid diversity and the end-Permian mass extinction. *Science* 325, 1118–1121.
- Brayard, A., Jenks, J.F., Bylund, K.G., the Paris Biota Team, 2019b. Ammonoids and nautiloids from the earliest Spathian Paris Biota and other early Spathian localities in southeastern Idaho, USA. *Geobios* 54, xxx–xxx.

- Brayard, A., Krümenacker L.J., Botting, J.P., Jenks, J.F., Bylund, K.G., Fara, E., Vennin, E., Olivier, N., Goudemand, N., Saucède, T., Charbonnier, S., Romano, C., Doguzhaeva, L., Thuy, B., Hautmann, M., Stephen, D.A., Thomazo, C., Escarguel, G., 2017. Unexpected Early Triassic marine ecosystem and the rise of the Modern evolutionary fauna. *Science Advances* 3, e1602159.
- Caze, B., Merle, D., Le Meur, M., Pacaud, J.-M., Ledon, D., Saint Martin, J.-P., 2011. Taxonomic implications of the residual colour patterns of ampullinid gastropods and their contribution to the discrimination from naticids. *Acta Palaeontologica Polonica* 56, 329–347.
- Caze, B., Merle, D., Schneider, S., 2015. UV light reveals the diversity of Jurassic shell colour patterns: Examples from the Cordebugle lagerstätte (Calvados, France). *Plos One* 10, e0126745.
- Charbonnier, S., Brayard, A., the Paris Biota Team, 2019. New thylacocephalans from the Early Triassic Paris Biota (Bear Lake County, Idaho, USA). *Geobios* 54, xxx–xxx.
- Chen, Z.-Q., Benton, M.J., 2012. The timing and pattern of biotic recovery following the end-Permian mass extinction. *Nature Geoscience* 5, 375–383.
- Doguzhaeva, L.A., Brayard, A., Goudemand, N., Krümenacker, L.J., Jenks, J.F., Bylund, K.G., Fara, E., Olivier, N., Vennin, E., Escarguel, G., 2018. An Early Triassic gladius associated with soft tissue remains from Idaho, USA – a squid-like coleoid cephalopod at the onset of Mesozoic Era. *Acta Palaeontologica Polonica* 63, 341–355.
- Edwards, N.P., Manning, P.L., Bergmann, U., Larson, P.L., van Dongen, B.E., Sellers, W.I., Webb, S.M., Sokaras, D., Alonso-Mori, R., Ignatyev, K., Barden, H.E., van Veelen, A., Anné, J., Egerton, V. M., Wogelius, R.A., 2014. Leaf metallome preserved over 50 million years. *Metallomics* 6, 774–782.
- Edwards, N.P., Webb, S.M., Krest, C.M., van Campen, D., Manning, P.L., Wogelius, R.A., Bergmann, U., 2018. A new synchrotron rapid-scanning X-ray fluorescence (SRS-XRF) imaging station at SSRL beamline 6-2. *Journal of Synchrotron Radiation* 25, 1565–1573.
- Falk, A.R., Kaye, T.G., Zhou, Z., Burnham, D.A., 2016. Laser fluorescence illuminates the soft tissue and life habits of the Early Cretaceous bird *Confuciusornis*. *Plos One* 11, e0167284.
- Galfetti, T., Bucher, H., Ovtcharova, M., Schaltegger, U., Brayard, A., Bruhwiler, T., Goudemand, N., Weissert, H., Hochuli, P.A., Cordey, F., Guodun, K.A., 2007. Timing

- of the Early Triassic carbon cycle perturbations inferred from new U-Pb ages and ammonoid biochronozones. *Earth and Planetary Science Letters* 258, 593–604.
- Garwood, R., Ross, A., Sotty, D., Chabard, D., Charbonnier, S., Sutton, M., Withers, P.J., 2012. Tomographic reconstruction of Neopteroous Carboniferous insect nymphs. *Plos One* 7, e45779.
- Goudemand, N., Romano, C., Leu, M., Bucher, H., Trotter, J.A., Williams, I.S., in press. Dynamic interplay between climate and marine biodiversity upheavals during the early Triassic Smithian-Spathian biotic crisis. *Earth-Science Reviews* (DOI: 10.1016/j.earscirev.2019.01.013).
- Gould, S.J., Calloway, C.B., 1980. Clams and brachiopods – ships that pass in the night. *Paleobiology* 6, 383–396.
- Grasby, S.E., Beauchamp, B., Embry, A., Sanei, H., 2013. Recurrent Early Triassic ocean anoxia. *Geology* 41, 175–178.
- Gueriau, P., Bernard, S., Bertrand, L., 2016. Advanced synchrotron characterization of paleontological specimens. *Elements* 12, 45–50.
- Gueriau, P., Jauvion, C., Mocuta, C., 2018. Show me your yttrium, and I will tell you who you are: implications for fossil imaging. *Palaeontology* 61, 981–990.
- Gueriau, P., Mocuta, C., Bertrand, L., 2015. Cerium anomaly at microscale in fossils. *Analytical Chemistry* 87, 8827–8836.
- Gueriau, P., Mocuta, C., Dutheil, D.B., Cohen, S.X., Thiaudière, D., the OT1 Consortium, Charbonnier, S., Clément, G., Bertrand, L., 2014. Trace elemental imaging of rare earth elements discriminates tissues at microscale in flat fossils. *PLoS One* 9, e86946.
- Haug, C., Haug, J. T., Waloszek, D., Maas, A., Frattigani, R., Liebau, S., 2009. New methods to document fossils from lithographic limestones of southern Germany and Lebanon. *Palaeontologia Electronica* 12, 12.3.6T, 12 p.
- Hone, D.W.E., Tischlinger, H., Xu, X., Zhang, F., 2010. The extent of the preserved feathers on the four-winged dinosaur *Microraptor gui* under ultraviolet light. *Plos One* 5, e9223.
- Iniesto, M., Thomazo, C., Fara, E., the Paris Biota Team, 2019. Deciphering the exceptional preservation of the Early Triassic Paris Biota (Bear Lake County, Idaho, USA). *Geobios* 54, xxx–xxx.
- Jauvion, C., Audo, D., Charbonnier, S., Vannier, J., 2016. Virtual dissection and lifestyle of a 165-million-year-old female polychelidan lobster. *Arthropod structure and development* 45, 122–132.

- Jattiot, R., Brayard, A., Fara, E., Charbonnier, S., 2015. Gladius-bearing coleoids from the Upper Cretaceous Lebanese Lagerstätten: diversity, morphology, and phylogenetic implications. *Journal of Paleontology* 89, 148–167.
- Kaye, T.G., Falk, A.R., Pittman, M., Sereno, P.C., Martin, L.D., Burnham, D.A., Gong, E., Xu, X., Wang, Y., 2015. Laser-Stimulated Fluorescence in Paleontology. *Plos One* 10, e0125923.
- Mapes, R.H., Landman, N.H., Klug, C., in press. Caught in the act? (Distraction sinking in ammonoid cephalopods). *Swiss Journal of Palaeontology* (DOI: 10.1007/s13358-018-0176-7).
- Moreau, J.-D., Néraudeau, D., Perrichot, V., Tafforeau, P., 2017. 100-million-year-old conifer tissues from the mid-Cretaceous amber of Charente (western France) revealed by synchrotron microtomography. *Annals of Botany* 119, 117–128.
- Orchard, M.J., 2007. Conodont diversity and evolution through the latest Permian and Early Triassic upheavals. *Palaeogeography, Palaeoclimatology, Palaeoecology* 252, 93–117.
- Payne, J.L., Lehrmann, D.J., Wei, J., Orchard, M.J., Schrag, D.P., Knoll, A.H., 2004. Large perturbations of the carbon cycle during recovery from the end-Permian extinction. *Science* 305, 506–509.
- Raup, D.M., 1979. Size of the Permo-Triassic bottleneck and its evolutionary implications. *Science* 206, 217–218.
- Reynard, B., Balter, V., 2014. Trace elements and their isotopes in bones and teeth: Diet, environments, diagenesis, and dating of archeological and paleontological samples. *Palaeogeography, Palaeoclimatology, Palaeoecology* 416, 4–16.
- Romano, C., Argyriou, T., Krumenacker L.J., the Paris Biota Team, 2019. Chondrichthyan teeth from the Early Triassic Paris Biota (Bear Lake County, Idaho, USA). *Geobios* 54, xxx–xxx.
- Sansonetti, M., Fanti, F., Thoury, M., Gueriau, P., Sciutto, G., Prati, S., 2017. Polychromatic UV-induced photoluminescence provides new insights into the fossilization of hard and soft tissues in Pescaria di Bolca fossils. 2017 International Workshop on Konservat-Lagerstätten.
- Saucède, T., Vennin, E., Fara, E., Olivier, N., the Paris Biota Team, 2019. A new holocrinid (Articulata) from the Paris Biota (Bear Lake County, Idaho, USA) highlights the high diversity of Early Triassic crinoids. *Geobios* 54, xxx–xxx.
- Sepkoski, J.J. Jr., 1981. A factor analytic description of the Phanerozoic marine fossil record. *Paleobiology* 7, 36–53.

- Simpson, G.G., 1926. Are *Dromatherium* and *Microconodon* mammals? *Science* 63, 548–549.
- Sutton, M.D., 2008. Tomographic techniques for the study of exceptionally preserved fossils. *Proceedings of the Royal Society of London B* 275, 1587–1593.
- Tafforeau, P., Boistel, R., Boller, E., Bravin, A., Brunet, M., Chaimanee, Y., Cloetens, P., Feist, M., Horszowska, J., Jaeger, J.-J., Kay, R.F., Lazzari, V., Marivaux, L., Nel, A., Nemoz, C., Thibault, X., Vignaud, P., Zabler, S., 2006. Applications of X-ray synchrotron microtomography for non-destructive 3D studies of paleontological specimens. *Applied Physics A* 83, 195–202.
- Thomazo, C., Brayard, A., Elmeknassi, S., Vennin, E., Olivier, N., Caravaca, G., Escarguel, G., Fara, E., Bylund, K.G., Jenks, J.F., Stephen, D.A., Killingsworth, B., Sansjofre, P., Cartigny, P., in press. Multiple sulfur isotope signals associated with the late Smithian event and the Smithian/Spathian boundary. *Earth-Science Reviews* (DOI: 10.1016/j.earscirev.2018.06.019).
- Thoury, M., Mille, B., Séverin-Fabiani, T., Robbiola, L., Réfrégiers, M., Jarrige, J.-F., Bertrand, L., 2016. High spatial dynamics-photoluminescence imaging reveals the metallurgy of the earliest lost-wax cast object. *Nature Communications* 7, 13356.
- Thuy, B., Escarguel, G., the Paris Biota Team, 2019. A new brittle star (Ophiuroidea: Ophiodermatina) from the Early Triassic Paris Biota (Bear Lake County, Idaho, USA). *Geobios* 54, xxx–xxx.
- Tischlinger, H., 2001. Die oberjurassischen Plattenkalke von Daiting. In: Weidert, W.K., (Ed.), *Klassische Fundstellen der Paläontologie*, 4. Goldschneck-Verlag, Korb, pp. 139–151.
- Tischlinger, H., Arratia, G., 2013. Ultraviolet light as a tool of investigating Mesozoic fishes with a focus on the ichthyofauna of the Solnhofen Limestone. In: Arratia, G., Schultze, H.-P., Wilson, M.V.H. (Eds.), *Mesozoic Fishes 5 – Global Diversity and Evolution*. Verlag Dr. F. Pfeil, München, pp. 549–560.
- Vermeij, G.J., 1977. The Mesozoic Marine Revolution: evidence from snails, predators and grazers. *Paleobiology* 3, 245–258.
- Wogelius, R.A., Manning, P.L., Barden, H.E., Edwards, N.P., Webb, S.M., Sellers, W.I., Taylor, K.G., Larson, P.L., Dodson, P., You, H., Da-qing, L., Bergmann, U., 2011. Trace metals as biomarkers for eumelanin pigment in the fossil record. *Science* 333, 1622–1626.

Figure captions

Fig. 1. A-C. Images of a caridean shrimp (slab UBGD 30553; Fig. S1, Appendix A) obtained under different illumination (Ill.)/detection(Det.) couples. **D.** False color RGB composite image of the same specimen. Each color corresponds to one of the A-C reflectance illumination/detection couples. The total length of the shrimp is ~15 mm.

Fig. 2. Articulated ophiuroid *Shoshonura brayardi* (UBGD 30565-1; Thuy et al., 2019) in ventral view. **A.** Photograph under visible light. **B.** Synchrotron μ XRF mapping image scanned at the DiffAbs beamline, SOLEIL (scan step: $50 \times 50 \mu\text{m}^2$, dwell time: 25 ms). Green color corresponds to strontium incorporated into the skeleton calcite highlighting the contours of the central disc (cd) and revealing the hidden termination of arms (a). Scale bar: 10 mm.

Fig. 3. Penaeoid shrimp (UBGD 30559) under visible light (**A**), UV light (**B**; 365 nm), and Synchrotron μ XRF mapping image (**C**) scanned at the DiffAbs beamline, SOLEIL (scan step: $50 \times 50 \mu\text{m}^2$, dwell time: 20 ms). Yellow color corresponds to yttrium incorporated into calcium phosphate; it appears concentrated near specific organs such as the digestive track of the individual (white arrows). Scale bar: 5 mm.

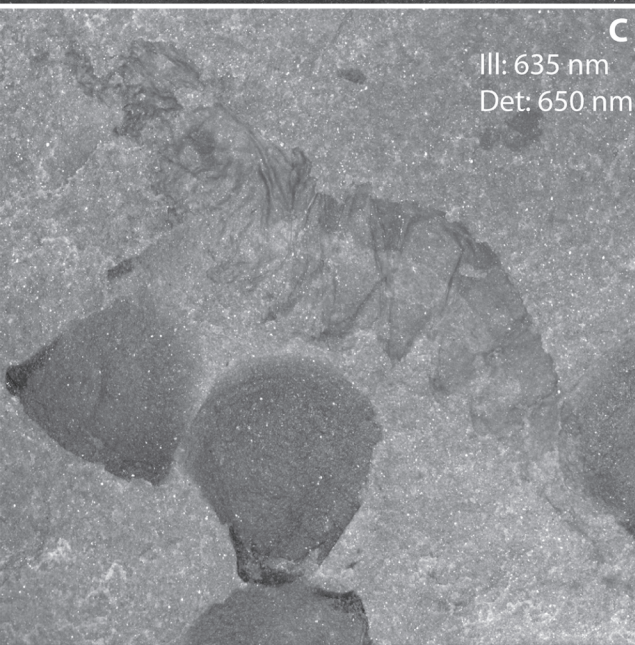
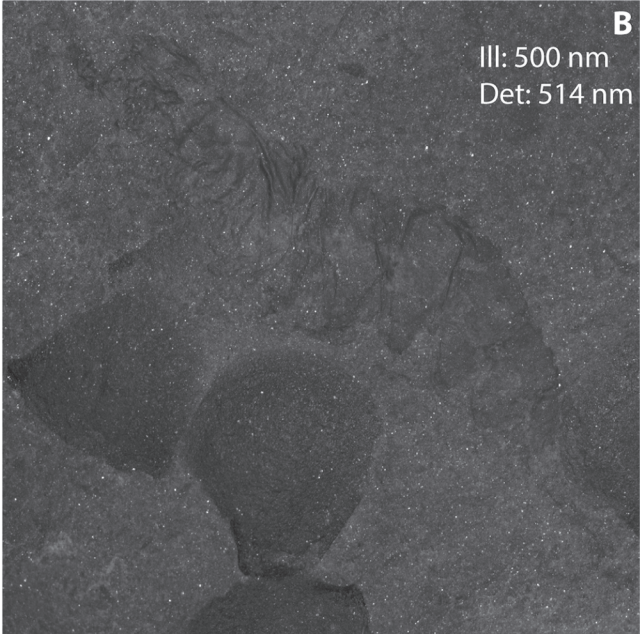
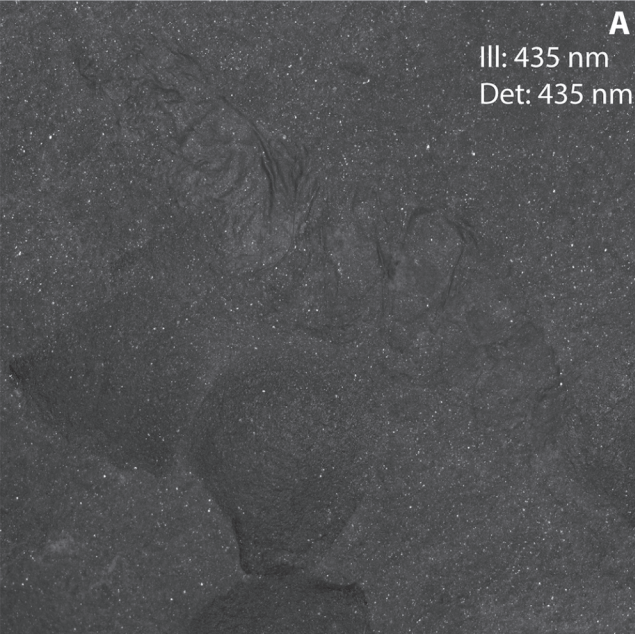
Fig. 4. False color RGB composite images obtained under different illumination/detection couples. **A.** Articulated specimen of the ophiuroid *Shoshonura brayardi* Thuy, 2019 (UBGD 30565-1; Fig. 2; Thuy et al., 2019). **B.** Proximal stem and cirri of the crinoid *Holocrinus* nov. sp. (UBGD 30612; Saucède et al., 2019). Each color corresponds to the following illumination/detection spectral ranges: A: blue – illumination 385 nm/detection 935 nm, green – illumination 460 nm/detection 935 nm, red – illumination 770 nm/detection 775 nm; B: blue – illumination 405 nm/detection 650 nm, green – illumination 460 nm/detection 935 nm, red – illumination 405 nm/detection 935 nm. Abbreviations: cd: central disc; ps: proximal stem; c: cirri. Scale bars: 5 mm.

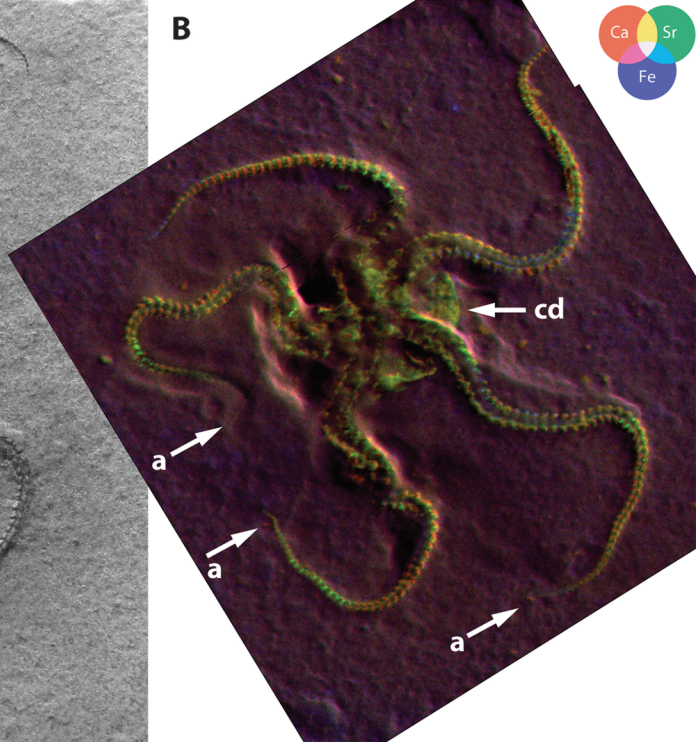
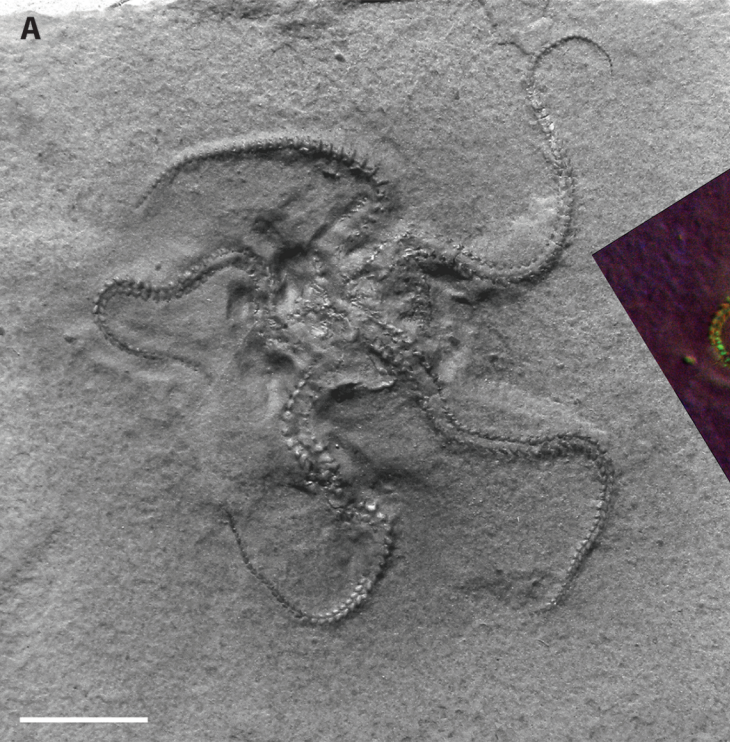
Fig. 5. A, C. Close-up views of slabs UBGD 30553 and UBGD 30679 under visible light, respectively (for specimen A, see also Fig. S1, Appendix A). **B, D.** Composite images of the same slabs obtained with different illumination/detection couples. B: the presence of several shrimp individuals (s) on the slab is hardly detectable under natural light (compare with A); D: the accumulation of cuticle remains (cr) and isolated appendages (a) surrounding poorly

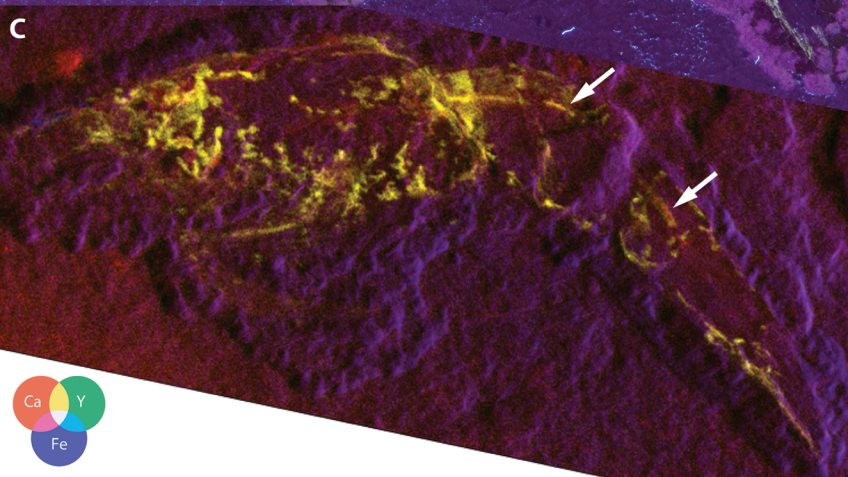
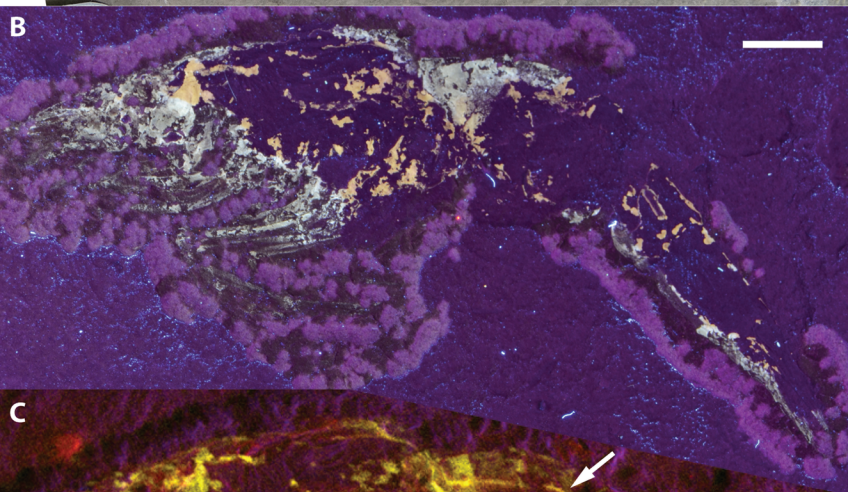
preserved shrimp specimens are barely perceptible under natural light (compare with C). Each color corresponds to the following illumination/detection spectral ranges: B: blue – illumination 405 nm/detection 650 nm, green – illumination 460 nm/detection 650 nm, red – illumination 525 nm/detection 650 nm; D: blue – illumination 385 nm/detection 571 nm, green – illumination 385 nm/detection 615 nm, red – illumination 385 nm/detection 792 nm. fs: fish scale. Size of the specimen at the top of picture B is ~20 mm.

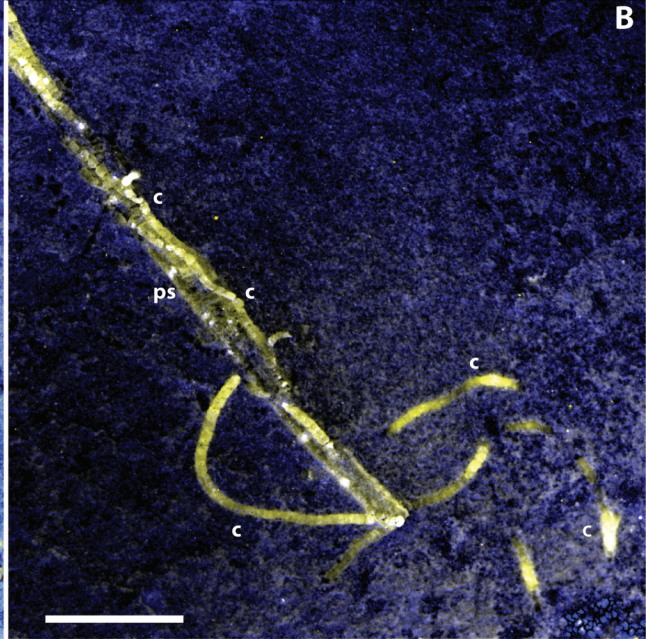
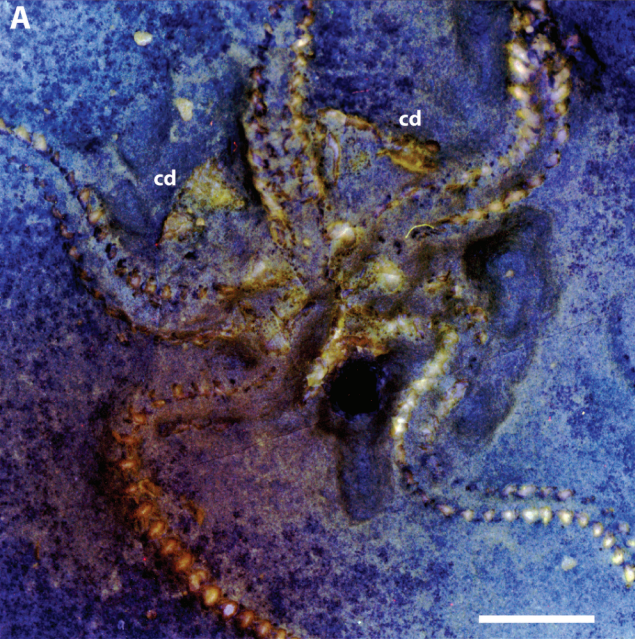
Fig. 6. Close-up view of caridean shrimps (slab UBGD 30553; Fig. S1, Appendix A) under the following illumination/detection couple: illumination 405 nm/detection 650 nm. Such an illumination/detection couple enhances fine anatomical details (e.g., smooth carapace, segments, delicate and short appendages) for these individuals. Length of the largest specimen is ~20 mm.

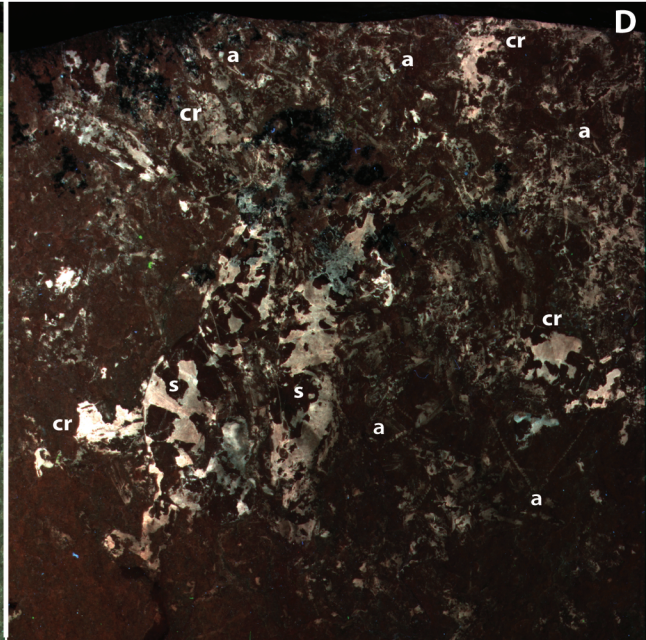
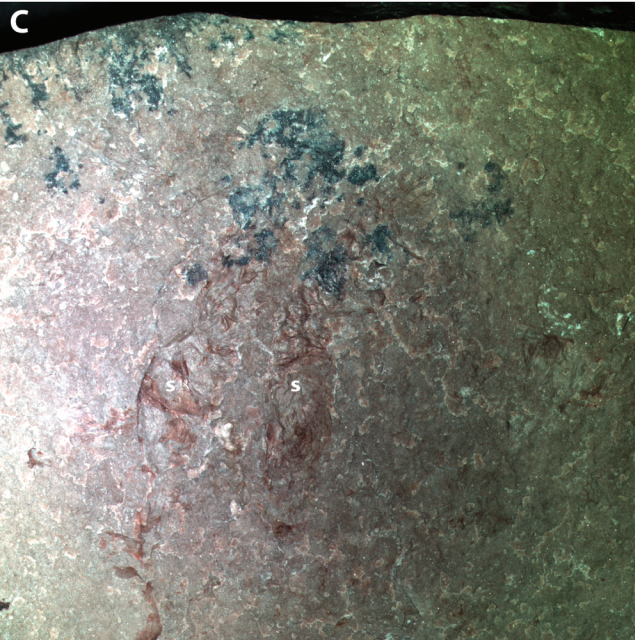
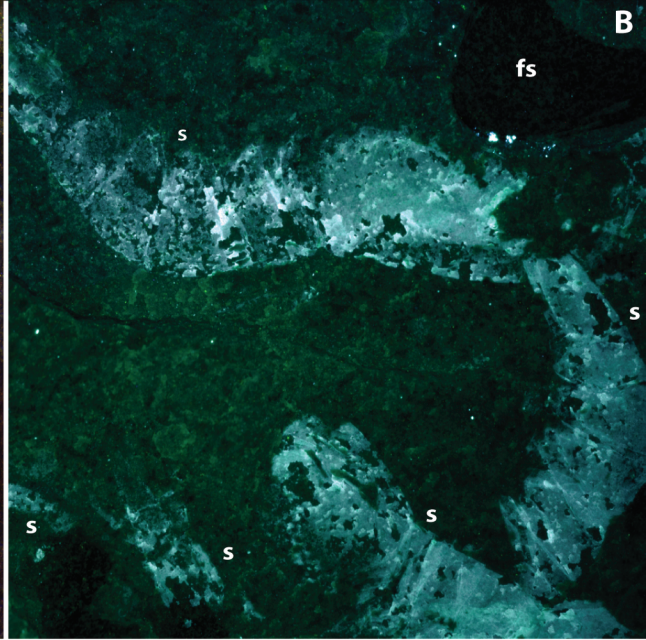
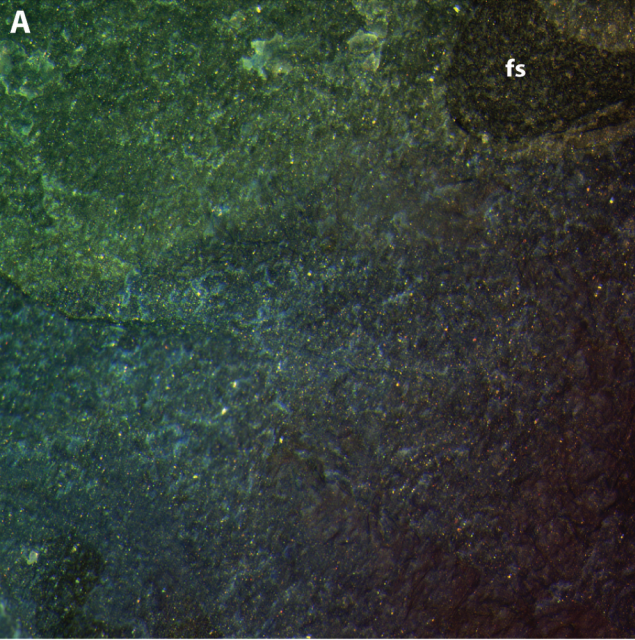
Fig. 7. A-C. Close-up view of caridean shrimps (slab UBGD 30553; Fig. S1, Appendix A) obtained under different illumination (Ill.)/detection(Det.) couples. **D.** False color RGB composite image of the same specimens. Each color corresponds to one of the A-C reflectance illumination/detection couples (A: green; B: red; C: blue). The composite image shows more contrasted anatomical details than under visible and UV lights. Length of the central specimen is ~15 mm.











Ill: 405 nm
Det: 650 nm

